

Novel Furin Inhibitors with Potent Anti-infectious Activity

Kornelia Harges,^[a] Gero L. Becker,^[a] Yinghui Lu,^[b] Sven O. Dahms,^[c] Susanne Köhler,^[d] Wolfgang Beyer,^[d] Kirsten Sandvig,^[e] Hiroyuki Yamamoto,^[f] Iris Lindberg,^[f] Lisa Walz,^[g] Veronika von Messling,^[g] Manuel E. Than,^[c] Wolfgang Garten,^[b] and Torsten Steinmetzer^{*,[a]}

New peptidomimetic furin inhibitors with unnatural amino acid residues in the P3 position were synthesized. The most potent compound 4-guanidinomethyl-phenylacteyl-Arg-Tle-Arg-4-amidinobenzylamide (MI-1148) inhibits furin with a K_i value of 5.5 μM . The derivatives also strongly inhibit PC1/3, whereas PC2 is less affected. Selected inhibitors were tested in cell culture for antibacterial and antiviral activity against infectious agents known to be dependent on furin activity. A significant protective effect against anthrax and diphtheria toxin was observed in the presence of the furin inhibitors. Furthermore,

the spread of the highly pathogenic H5N1 and H7N1 avian influenza viruses and propagation of canine distemper virus was strongly inhibited. Inhibitor MI-1148 was crystallized in complex with human furin. Its N-terminal guanidinomethyl group in the *para* position of the P5 phenyl ring occupies the same position as that found previously for a structurally related inhibitor containing this substitution in the *meta* position, thereby maintaining all of the important P5 interactions. Our results confirm that the inhibition of furin is a promising strategy for a short-term treatment of acute infectious diseases.

Introduction

Furin belongs to the family of proprotein convertases (PC), which comprises nine members in humans. Furin and the other six furin-like proteases, PC1/3, PC2, PACE4, PC4, PC5/6, and PC7, cleave their substrates after paired, and in rare cases after single, basic residues. The preferred cleavage motif of furin substrates is Arg-Xaa-(Lys/Arg)-Arg↓Xaa, containing an

additional Arg residue in the P4 position. In contrast, the other two PCs, SKI-1 and PCSK9, prefer paired hydrophobic residues in the P1 and P2 positions.^[1,2]

Furin is a type I transmembrane serine protease and is ubiquitously expressed in vertebrates and invertebrates. The protein cycles from the *trans*-Golgi network (TGN) through the endosomal system to the cell membrane and back. The physiological function of furin is the activation of precursor forms of numerous receptors, hormones, and cell surface proteins. Studies with furin knockout mice revealed that furin expression is critical to embryogenesis. The complete knockout of the *fur* gene is not tolerated and results in embryonic death at day 11.^[3,4] In contrast, mice with a liver-specific conditional furin knockout are viable, which suggests sufficient redundancy between the furin-like PCs in adulthood.^[5] In addition, the specific inhibition of furin by polyarginine inhibitors is well tolerated in adult animals.^[6,7] Besides its physiological functions, furin also contributes to the pathology of numerous diseases. It activates certain viral and bacterial pathogenic proteins and is involved in tumorigenesis, atherosclerosis, and diabetes as well as neurodegenerative disorders.^[1,2,8]

Several viruses possess fusogenic surface glycoproteins that are cleaved and thereby activated by furin or related PCs. Examples are the precursors of fusion proteins of *Orthomyxoviridae* (e.g., influenza virus), *Paramyxoviridae* (e.g., measles, canine distemper virus), *Filoviridae* (Ebola and Marburg virus), and *Flaviviridae* (e.g., dengue, West Nile virus).^[9] Furthermore, furin activates various bacterial toxins including the protective antigen (PA) precursor of anthrax toxin secreted by *Bacillus anthracis*. Furin also cleaves and thereby activates diphtheria toxin, *Pseudomonas* exotoxin A (PEA), and shiga toxin. Therefore, the inhibition of furin could be a suitable approach for the development of new short-term therapies in acute infec-

[a] Dr. K. Harges, Dr. G. L. Becker, Prof. T. Steinmetzer
Institute of Pharmaceutical Chemistry, Philipps University
Marbacher Weg 6, 35032 Marburg (Germany)
E-mail: steinmetzer@uni-marburg.de

[b] Dr. Y. Lu, Prof. W. Garten
Institute of Virology, Philipps University
Hans-Meerwein-Strasse 2, Marburg (Germany)

[c] Dr. S. O. Dahms, Dr. M. E. Than
Protein Crystallography Group
Leibniz Institute for Age Research—Fritz Lipmann Institute (FLI)
Beutenbergstrasse 11, 07745 Jena (Germany)

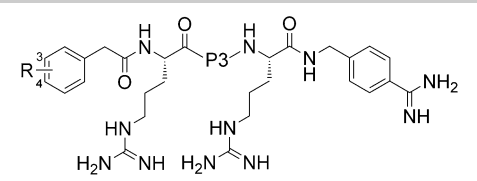
[d] S. Köhler, Dr. W. Beyer
Institute of Environmental and Animal Hygiene, University of Hohenheim
Garbenstrasse 30, 70599 Stuttgart (Germany)

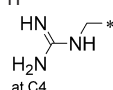
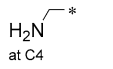
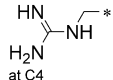
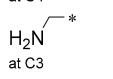
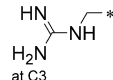
[e] Prof. K. Sandvig
Department of Biochemistry and Centre for Cancer Biomedicine
Institute for Cancer Research, The Norwegian Radium Hospital
Montebello, 0310 Oslo (Norway)

[f] Dr. H. Yamamoto, Prof. I. Lindberg
Department of Anatomy and Neurobiology, University of Maryland
Baltimore, Maryland 21201 (USA)

[g] L. Walz, Dr. V. von Messling
Veterinary Medicine Division, Paul-Ehrlich-Institute
Federal Institute for Vaccines and Biomedicines
Paul-Ehrlich-Strasse 51–59, 63225 Langen (Germany)

 Supporting Information for this article is available on the WWW under <http://dx.doi.org/10.1002/cmdc.201500103>. It contains a scheme for the synthesis of inhibitor **9**, the ¹H NMR and ¹³C NMR spectra of inhibitors **18** and **19**, cytotoxicity assay with selected inhibitors in MDCK cells, and the synthesis of the fluorogenic substrate Phac-Arg-Val-Arg-Arg-AMC.

Table 1. Analytical characterization of the inhibitors and their potency against furin, PC1/3, and PC2.


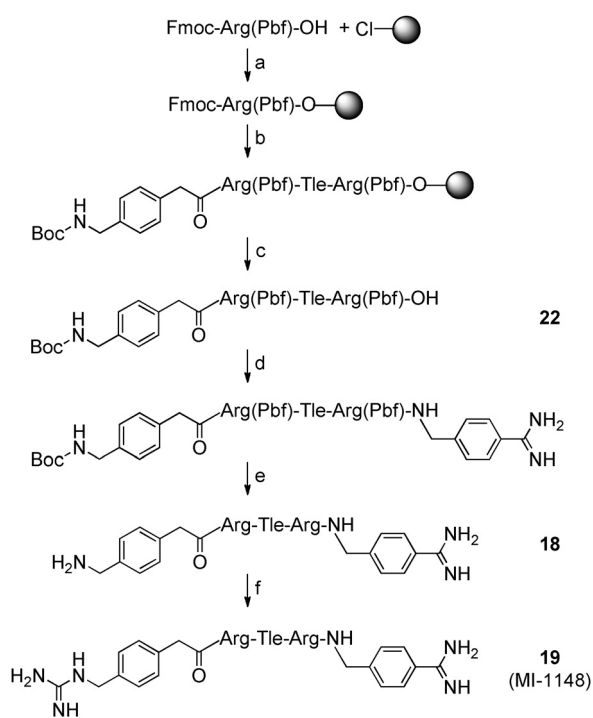
| No. | R | P3 | HPLC [min] | MS | | K_i [nM] ^[a] furin | Residual activity [%] ^[a] | | |
|--------------------------------|---|-------|------------|-------|----------------------|------------------------------------|--------------------------------------|------------------|---------------------|
| | | | | calcd | found | | PC1/3 at 1 μ M | at 0.1 μ M | PC2 at 1 μ M |
| 1 ^[b] | H | Gly | 21.4 | 636.4 | 319.3 ^[c] | 44.3 \pm 6.0 | 80.6 \pm 1.6 | – ^[d] | 86.5 \pm 3.7 |
| 2 ^[b] | H | Ala | 21.8 | 650.4 | 326.4 ^[c] | 18.2 \pm 1.5 | 61.2 \pm 1.8 | – ^[d] | 74.8 \pm 2.4 |
| 3 ^[b] | H | Val | 24.4 | 678.4 | 679.4 | 0.66 \pm 0.22 | 7.4 \pm 0.4 | 27.1 \pm 0.8 | 62.9 \pm 1.1 |
| 4 ^[b] | H | Leu | 27.5 | 692.4 | 347.3 ^[c] | 7.95 \pm 0.09 | 46.6 \pm 3.0 | – ^[d] | 78.0 \pm 0.9 |
| 5 ^[b] | H | Ile | 27.1 | 692.4 | 347.3 ^[c] | 0.67 \pm 0.25 | 3.9 \pm 0.3 | 16.3 \pm 1.3 | 73.8 \pm 2.2 |
| 6 | H | Aib | 22.3 | 664.4 | 333.3 ^[c] | 408 \pm 55.3 | 87.6 \pm 1.0 | – ^[d] | 97.6 \pm 2.1 |
| 7 | H | 1-Adg | 32.7 | 770.5 | 771.5 | 64.7 \pm 2.3 | 84.9 \pm 2.6 | – ^[d] | 93.0 \pm 4.0 |
| 8 | H | 2-Abu | 23.0 | 664.4 | 333.2 ^[c] | 2.06 \pm 0.83 | 36.7 \pm 1.2 | – ^[d] | 85.4 \pm 1.9 |
| 9 | H | Tle | 26.8 | 692.4 | 347.4 ^[c] | 0.17 \pm 0.04 | 1.4 \pm 0 | 9.3 \pm 0.4 | 52.6 \pm 1.5 |
| 10 | H | Tba | 28.8 | 706.4 | 354.3 ^[c] | 1.98 \pm 0.63 | 17.4 \pm 0.8 | – ^[d] | 87.6 \pm 2.4 |
| 11 | H | Nva | 25.1 | 678.4 | 679.3 | 3.67 \pm 1.1 | 40.2 \pm 3.1 | – ^[d] | 90.6 \pm 1.7 |
| 12 | H | Cpa | 26.0 | 690.4 | 691.4 | 1.83 \pm 0.08 | 23.6 \pm 1.0 | – ^[d] | 77.5 \pm 3.6 |
| 13 | H | Cha | 32.2 | 732.5 | 733.4 | 7.13 \pm 0.93 | 68.0 \pm 2.9 | – ^[d] | 90.9 \pm 4.9 |
| 14 | H | Nle | 27.7 | 692.4 | 693.6 | 6.16 \pm 2.68 | 51.3 \pm 1.8 | – ^[d] | 86.8 \pm 3.3 |
| 15 | H | Pen | 25.3 | 710.4 | 711.2 | 0.25 \pm 0.01 | 2.8 \pm 0.2 | 17.3 \pm 1.8 | 64.8 \pm 1.0 |
| 16 | H | Chg | 28.9 | 718.4 | 719.5 | 7.14 \pm 0.47 | 34.8 \pm 0.2 | – ^[d] | 89.5 \pm 0.8 |
| 17 ^[b] (MI-0701) |  | Val | 19.7 | 749.5 | 375.9 ^[c] | 0.0076 \pm 0.0013 ^[e] | 1.3 \pm 0.1 | 6.4 \pm 0.9 | 35.5 \pm 1.0 |
| 18 |  | Tle | 19.1 | 721.5 | 722.4 | 0.0224 \pm 0.0021 ^[e] | 0.9 \pm 0.5 | 4.2 \pm 0.8 | 63.8 \pm 2.4 |
| 19 (MI-1148) |  | Tle | 20.4 | 763.5 | 764.3 | 0.0055 \pm 0.0003 ^[e] | 0.9 \pm 0.6 | 2.9 \pm 0.6 | 27.1 \pm 1.2 |
| 20 |  | Tle | 19.8 | 721.5 | 722.4 | 0.0361 \pm 0.0001 ^[e] | 2.0 \pm 0.2 | 13.3 \pm 0.4 | 64.7 \pm 5.4 |
| 21 |  | Tle | 20.3 | 763.5 | 764.3 | 0.0068 \pm 0.0005 ^[e] | 1.1 \pm 0.7 | 5.2 \pm 0.7 | 38.2 \pm 1.1 |

[a] Data represent the mean \pm SD obtained for at least three independent measurements. [b] These compounds were previously published.^[20,22]
[c] $[M+2H]^{2+} - 2$. [d] Not determined. [e] K_i values were determined under tight-binding conditions.

plains small differences with our previous data, for which, for instance, a K_i value of 40 nM was determined for this Gly inhibitor.^[22]

All compounds were synthesized according to a previously described strategy,^[17,22] and their analytical data are summarized in Table 1. Briefly, the protected P5–P2 segment was prepared on 2-chlorotritylchloride resin with a standard 9-fluorenylmethoxycarbonyl (Fmoc) solid-phase peptide synthesis (SPPS) protocol. This segment was cleaved under mild acidic conditions from the resin, maintaining the side chain protection, followed by coupling of 4-aminobenzylamine-2HCl in solution, and then final removal of all protecting groups. In the case of inhibitors with an N-terminal aminomethylphenyl-acetyl residue, the final conversion into the analogous guanidinomethyl derivative was performed by treatment with commercially available 1H-pyrazole-1-carboxamide-HCl^[24] (Scheme 2).

The addition of the first methyl group provided Ala inhibitor **2**; its potency was improved by a factor of roughly two relative to that of inhibitor **1**. Addition of the subsequent methyl group had the strongest positive influence; a nearly 10-fold improvement in the inhibition constant (2.06 nM) was achieved by the incorporation of 2-Abu (**8**), which lacks only one terminal methyl group in comparison to Val. In contrast, the incorporation of the sterically hindered C α -dialkylated Aib residue resulted in a dramatic drop in affinity. Further elongation of the 2-Abu side chain by incorporation of norvaline (Nva, **11**) or noleucine (Nle, **14**) reduced the affinity, whereas the addition of a second methyl group at the C β -atom provided three-times more potent Val inhibitor **3**. A nearly identical affinity was found for Ile inhibitor **5**, which confirmed our previous results.^[22] Going from Nva to the C γ -branched Leu clearly reduced efficacy, whereas potency was restored both by cyclization of the Leu side chain leading to cyclopropylalanine (Cpa)



Scheme 2. Synthesis of inhibitors **18** and MI-1148 (**19**). a) Loading of 2-chlorotriyl chloride resin with Fmoc-Arg(Pbf)-OH, DIPEA (4 equiv), dry CH_2Cl_2 , 2 h; b) Fmoc-SPPS, double couplings with the amino acid or Boc-aminomethylphenylacetic acid (4 equiv), HBTU (4 equiv), HOBT (4 equiv) and DIPEA (8 equiv); c) cleavage from the resin with 1% TFA in CH_2Cl_2 (3 \times) for 30 min and removal of the solvent in vacuo; d) 4-amidinobenzylamine-2HCl (1.5 equiv), PyBOP (1.7 equiv), 6-Cl-HOBT (4.5 equiv), and DIPEA (10 equiv) in DMF, 2 h; e) removal of the protecting groups with TFA/TIS/ H_2O (95:2.5:2.5 v/v/v), 3 h, precipitation in cold diethyl ether, purification by preparative HPLC; f) 1H-pyrazole-1-carboxamidinium-HCl (5 equiv) in 1 M Na_2CO_3 , 24 h. All final compounds were purified by reverse-phase preparative HPLC and were obtained as lyophilized TFA salts.

inhibitor **12** and by incorporation of *tert*-butylalanine (Tba, **10**). To our delight, relative to Val inhibitor **3**, nearly fourfold stronger furin inhibition was obtained for Tle derivative **9**, which contains a space-filling quaternary $\text{C}\beta$ -atom at the P3 side chain. As a close analogue of Tle, penicillamine was also introduced and provided similarly potent inhibitor **15**. Moreover, the mercapto group of this inhibitor could serve as a handle for further modifications, for example, by alkylation. A strong drop in affinity was obtained after incorporation of hydrophobic 1-adamantylglycine (**7**), although this residue also contains a quaternary $\text{C}\beta$ -atom. Reduced potency similar to that found for Leu inhibitor **4** was obtained for Cha analogue **13** and Chg derivative **16**.

On the basis of these results, four additional inhibitors were prepared by combining the preferred Tle residue with the basic-substituted phenylacetyl residues in the P5 position (Table 1). As described for Val analogue **17** (MI-0701),^[20] all of these Tle derivatives possess very strong affinity against furin and were characterized as tight-binding inhibitors. Relative to potency of the P5 aminomethyl-substituted derivatives, a higher potency in the single digit picomolar range was found for the P5 guanidinomethyl analogues. Although the K_i

value for most-potent inhibitor **19** [$(5.5 \pm 0.3) \mu\text{M}$] was slightly improved relative to that of Val analogue **17**, the difference in the inhibition constants is less than that of the inhibitors with a neutral P5 residue.

Moreover, these inhibitors were also tested against the related proteases PC1/3 and PC2. Owing to the limited amount of available enzyme, only residual activities, at constant inhibitor concentrations of $1 \mu\text{M}$, were determined. As expected on the basis of previous studies,^[20] strong inhibition of PC1/3 was found, especially for the inhibitors containing a basic-substituted P5 residue. With all compounds showing less than 10% residual activity, additional measurements at a 10-fold reduced inhibitor concentration were performed. A strong correlation between furin and PC1/3 inhibition was found. Within the proteinogenic residues, Val and Ile were preferred by PC1/3, whereas a slight preference for Ile was found. A similar potency was obtained for penicillamine analogue **15**, and nearly twofold stronger PC1/3 inhibition was determined for Tle inhibitor **9**. Improved affinity was found for derivatives with basic P5 groups; compound **19** is also the most potent PC1/3 inhibitor. A relatively weak affinity was observed against PC2. For best compound **19**, a residual activity of approximately 27% was determined at a concentration of $1 \mu\text{M}$, although only a minor improvement was found after incorporation of basic P5 residues. Owing to its preferred potency for furin among the PCs tested, the structure of inhibitor MI-1148 (**19**) in complex with furin was determined.

Crystallization of human furin in complex with MI-1148 (**19**)

Initial furin crystals in complex with the previously described inhibitor I-1 (3-guanidinomethyl-Phac-Arg-Val-Arg-4-amba, $K_i = 8 \mu\text{M}$)^[20] were grown, and the inhibitor was exchanged with tighter binding analogue **19**, essentially as described before.^[21] The complex crystals diffracted up to 2.15 Å resolution by using synchrotron radiation and gave rise to a dataset of good quality (Table 2). Refinement of the structure resulted in final R/R_{free} factors of 18.6/21.9% with 95.3% of the residues in the most favored regions, 4.7% in the allowed regions, and 0% in disallowed regions of the Ramachandran plot^[25] and good stereochemistry.

The occupancy of the novel inhibitor within the highly negatively charged active site cleft of all six molecules within the asymmetric unit of the orthorhombic crystals was confirmed by a strong difference electron density, which clearly showed the molecular variations between compound **19** and the initially cocrystallized analogue I-1, as described below (Figure 1 A). Correspondingly, complete exchange of the inhibitor was achieved, as expected from the extended soaking procedure.

Inhibitor **19** structurally varies from I-1 at two positions; the P3 residue is Tle instead of the proteinogenic Val, and the guanidinomethyl substitution at the P5 phenyl ring resides at the *para* position instead of the *meta* position. Correspondingly and as expected, the overall binding of inhibitor **19** is very similar to that of I-1 (Figure 1 A).^[21] The tetrabasic inhibitor is complementary in charge to the strongly acidic catalytic cleft. Its

Table 2. Data collection and refinement statistics (PDB-ID: 4RYD).

| Data collection statistics | |
|---|-------------------------|
| Wavelength [Å] | 0.918 |
| Unit cell parameters | $P2_12_12_1$ |
| a, b, c [Å] | 141.65, 152.70, 168.40 |
| Resolution range ^[a] [Å] | 50.0–2.15 (2.28–2.15) |
| R_{merge} ^[a] [%] | 13.5 (69.3) |
| I/σ ^[a] | 9.1 (2.0) |
| Completeness ^[a] [%] | 98.3 (97.7) |
| Observations: total/unique | 669 363/194 799 |
| Refinement statistics | |
| Resolution range ^[a] [Å] | 50.0–2.15 (2.25–2.15) |
| $R_{\text{work}}/R_{\text{free}}$ | 18.6 (26.8)/21.9 (30.7) |
| Non-hydrogen atoms, total | 23 774 |
| Protein/inhibitor/other | 21 332/330/2 112 |
| B factors [Å ²] | |
| Overall/Wilson plot | 26.0/29.9 |
| Protein/inhibitor/other | 25.3/21.4/33.8 |
| RMSD bond length [Å] | 0.0076 |
| RMSD bonded B-factors [Å ²] | 2.41 |

[a] Highest resolution shell is given in parentheses.

P1 4-amba residue inserts deeply into the S1 pocket, where it forms tight hydrogen bonds with the furin residues and through bridging water molecules also contacts the PC-specific Ca-2 ion.^[21] The P2 side chain interacts predominantly with Asn192 and Asp154 of the furin surface. Furthermore, two strong β -sheet-like H-bonds between the carbonyl groups and the amide groups of the P3 Tle residue and Gly255 of furin contribute to inhibitor binding, and the extended hydrogen-bonding network at the joined S4/S5 pocket is basically retained. Interestingly, the 4-guanidinomethyl group at the P5 phenyl ring makes similar strong hydrogen bonds with the main-chain carbonyl group of Val231, the side-chain carboxylate group of Glu236, and to the conserved bridging water molecule #58, which in turn provides identical contacts to Asp233, Glu236, and Ala267 of the protein surface, as observed for the complex with I-1.^[21] As a consequence, the phenyl ring of the P5 residue shifts towards the protein surface by approximately 1 Å (Figure 1B).

Replacement of the P3-Val residue in I-1 with the more bulky Tle residue in inhibitor **19** does not result in any major conformational alterations. Two of its three side-chain methyl groups are oriented similarly to that observed for P3-Val (Figure 1C). A slight counterclockwise horizontal rotation (basically towards the viewer) of the P3 moiety by roughly 5° results, however, in a shift of these two methyl groups by approximately 0.5–0.8 Å, which possibly gives rise to stronger van der Waals contacts with the phenyl ring of P1 and C γ of Glu257. The third methyl group also makes van der Waals contacts with the inhibitor backbone, mainly with the amide hydrogen atom, but also with the carbonyl oxygen atom of P2. Correspondingly, the P3-Tle moiety seems to fit better into the triangular crevice formed by the phenyl ring of P1, the inhibitor backbone, and the Glu257 side chain of the protein. The differences in contact are, however, small, and the observed posi-

tional shifts of the two methyl groups are almost within the error of crystallographic structures, such that no final conclusions can be drawn as to the structural reason for the observed gain in affinity of P3-Tle relative to that of P3-Val.

Binding of noncovalent inhibitors to human furin stabilizes the enzyme

To compare the inhibitory strength of various inhibitors with the conformational stability of the respective inhibitor–enzyme complexes, we determined their melting temperature, T_m , in respective thermofluor assays.^[26] Plotting T_m as a function of pK_i , we observed a clear correlation (Figure 2), which suggests a similar binding mode for these inhibitors. However, there are small deviations from linearity with these inhibitors. This is readily explained, as not all contacts that increase the interaction between a given inhibitor and the enzyme, which thus lowers the K_i , do so at the same time and to the same extent also stabilize the enzyme–inhibitor complex. In general, however, a tighter binding inhibitor results in higher T_m and increased conformational stability and hence better crystallizability of the respective inhibitor–enzyme complexes.^[21] The determination of T_m can, however, only be suggestive for inhibitory constants and does not replace their measurement.

Antibacterial and antiviral activities in cell culture

We previously demonstrated an inhibitory effect of selected compounds on the propagation of highly pathogenic avian influenza virus (HPAIV) in Madin–Darby canine kidney (MDCK) cells by using the H7N1 fowl plague virus (FPV) strain and analyzed their protective effect on Vero cells against intoxication by shiga toxin. In the present study, we investigated the influence of our new inhibitors on the protection of cells against anthrax and diphtheria toxin and analyzed the propagation of the canine distemper virus wildtype strain 5804PeH^[27] as well as the spread of two HPAIV strains, including FPV and H5N1 KAN-1, in cell culture.

Inhibition of anthrax toxin action

Anthrax is a serious bacterial infection caused by *Bacillus anthracis* and primarily affects herbivores.^[28] The secreted anthrax toxins are bipartite toxins consisting of the protective antigen (PA) and either the edema factor (EF) or the lethal factor (LF). The intoxication process begins with the binding of the precursor protein PA₈₃ to specific receptors on the cell surface. PA₈₃ contains a multibasic sequence that is cleaved by furin or furin-like PCs.^[29] The activated PA then forms a heptameric complex, which can bind up to three molecules of LF and/or EF and is then internalized by clathrin-mediated endocytosis. In the acidic endosomes, this complex forms a pore and enables the translocation of LF and EF into the cytosol. LF is a Zn²⁺ protease that cleaves and thereby inactivates mitogen-activated protein (MAP) kinase kinases, which leads to lethal disruption of the MAP kinase signaling pathway. EF is a Ca²⁺- and calmodulin-dependent adenylate cyclase that mediates

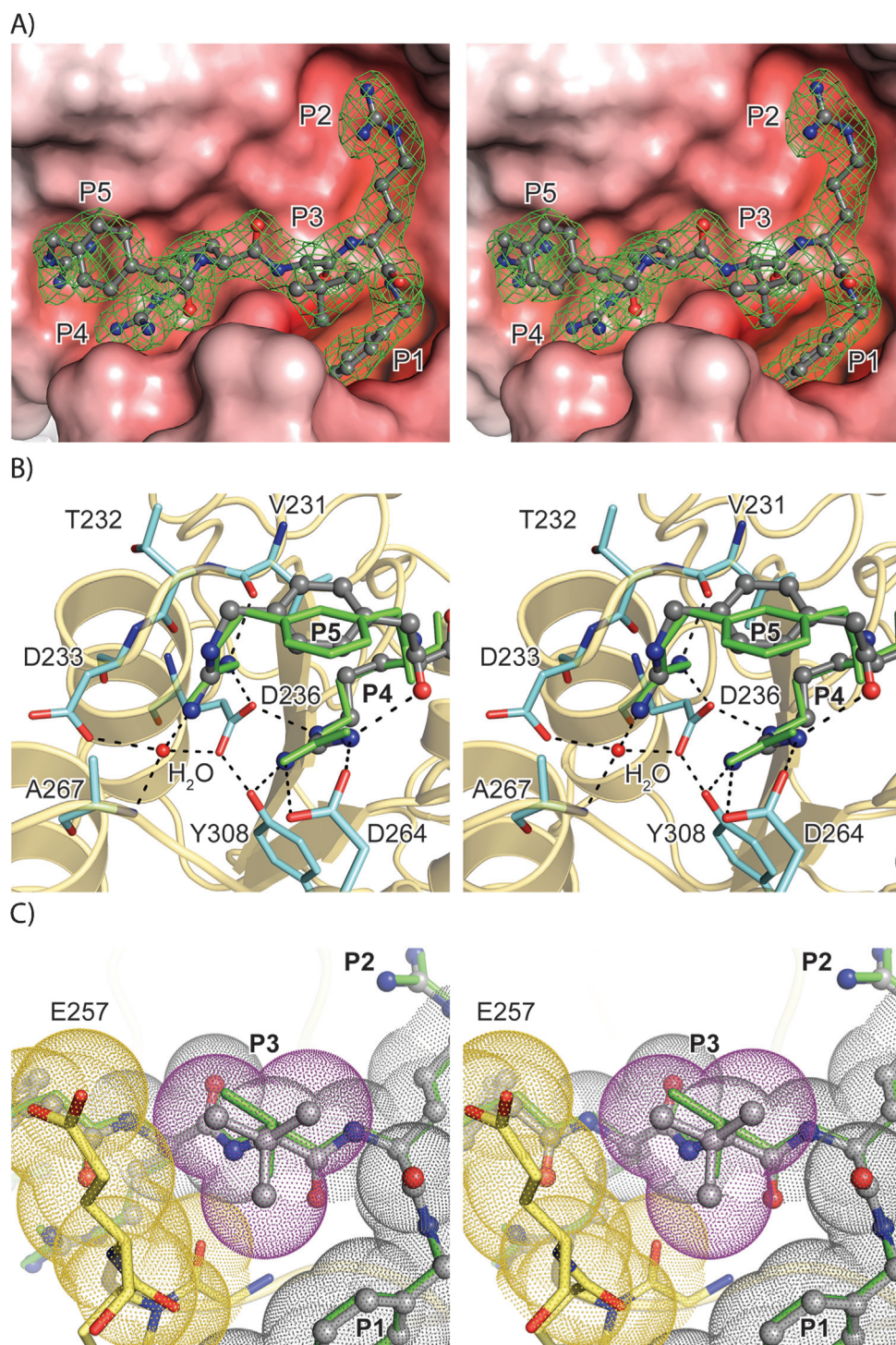


Figure 1. Structure of human furin in complex with 4-guanidinomethyl-phenylacetyle-Arg-Tle-Arg-4-amidinobenzylamide (MI-1148, **19**). A) Stereo representation of the active site cleft (surface representation) with bound inhibitor as a ball-and-stick model in gray. The molecular surface was colored by the calculated electrostatic potential ranging from -20 kTe^{-1} (red) to $+20 \text{ kTe}^{-1}$ (blue). The residues of the inhibitor are numbered (P1–P5) and its kicked Fo–Fc difference electron density omit map (green mesh) is contoured at 3.5σ . B) In the stereo panels, the $\text{C}\alpha$ carbon trace of the protease is given as a cartoon representation (pale yellow). The inhibitor is shown in dark gray (ball-and-stick model), and the important furin residues are shown in cyan (stick model). Selected water molecules are shown as red spheres. Important interactions are highlighted with black dashes. The aligned structure of I-1 (3-guanidinomethyl-Phac-Arg-Val-Arg-4-amba) bound to furin (PDB-ID: 4OMC⁽²¹⁾) is given as stick model in green. C) Stereo representation of the space-filling properties of the Tle residue at the P3 position. The inhibitor is shown in dark gray (ball-and-stick model) and the important furin residues are shown in yellow (cartoon, stick model). The van der Waals radii of selected atoms are illustrated by dotted spheres. Yellow dots belong to protein atoms, gray dots to inhibitor atoms, and magenta dots to side-chain atoms of Tle at P3. The superimposed structure of I-1 bound to furin (PDB-ID: 4OMC⁽²¹⁾) is given as a stick model in green.

the intracellular increase of cyclic adenosine monophosphate (cAMP), which leads to edema formation.^[30] Therefore, inhibition of furin-mediated PA activation might represent a supplemental approach to the conventional therapy against anthrax of antibiotics or the recently approved antibody Raxibacumab.^[31,32]

To test the protective effect of selected inhibitors against anthrax toxin, macrophages were treated with constant concentrations of PA and LF in the presence of various inhibitors, whereby D9R ($K_i = 1.3 \text{ nM}$ against furin)^[15] served as a reference (Figure 3). At concentrations between 0.05 and $100 \mu\text{M}$, the inhibitors showed no cytotoxic effects. Surprisingly, only a weak effect was obtained for the reference D9R, although significant protection was found in a previous study.^[15] Strong and concentration-dependent protection was found for all other compounds. The highest efficacy was produced by inhibitors **17**, **21**, and **19**, all containing a guanidinomethyl substitution at the P5 phenyl ring. These data reveal a clear correlation between the K_i values against furin and the protective effects in cell culture.

Inhibition of diphtheria toxin action

Corynebacterium diphtheriae can cause severe infections in humans, especially in children and older people. This may lead to complications such as myocarditis and peripheral neuropathy.^[33] Experiments in cell culture revealed that furin cleaves diphtheria toxin between Arg193 and Ser194 into two fragments, called A and B, linked by a disulfide bridge, and thereby activates it.^[34] Fragment A inhibits protein biosynthesis by adenosine diphosphate (ADP)-ribosylation of elongation factor 2,

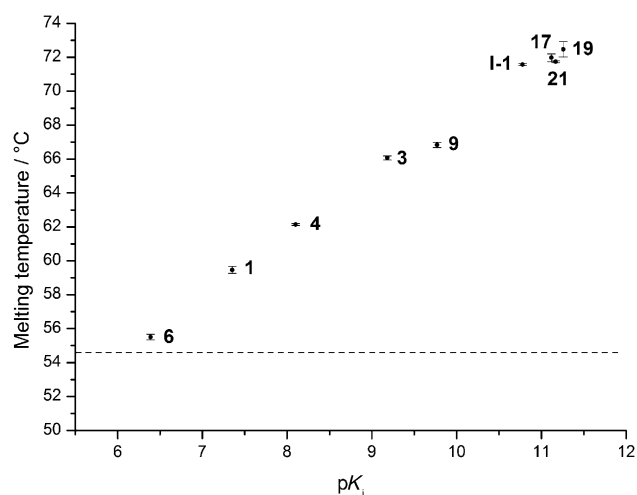


Figure 2. Gain of global structural stability as a function of inhibitory strength. Melting temperatures were determined on the basis of the fluorescence of the dye Sypro Orange by stepwise heating. The mean $T_m \pm SD$ resulting from three independent measurements is given for each inhibitor as a function of K_i in a semilogarithmic plot. The horizontal dashed line represents the T_m of the uninhibited enzyme at $(54.6 \pm 0.0)^\circ\text{C}$.

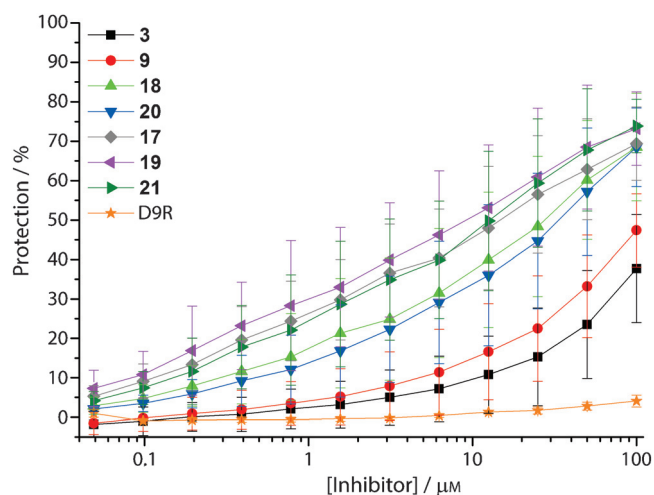


Figure 3. Protection of murine macrophages against anthrax toxin by selected inhibitors ($n=3$), determined by MTT assay. Cells were treated with 500 ng mL^{-1} PA and 100 ng mL^{-1} LF in the presence of various concentrations of inhibitors.

which is responsible for the guanosine triphosphate (GTP)-dependent translocation step on the ribosome.

Therefore, we screened selected inhibitors at a constant concentration of 100 nM against unnicked diphtheria toxin in Vero cells. In this cell line, we also observed no cytotoxic effect at the inhibitor concentrations used. We determined a protective factor by calculating the ratio of the required toxin concentrations inducing 50% cell death in the presence of the inhibitors relative to the control without inhibitor (Figure 4A).

Only negligible protection was found in the presence of D9R (protective factor 1.12 ± 0.19). An approximately twofold improved effect was achieved with inhibitors **3** and **9**, both containing a neutral P5 residue. All inhibitors with basic P5 resi-

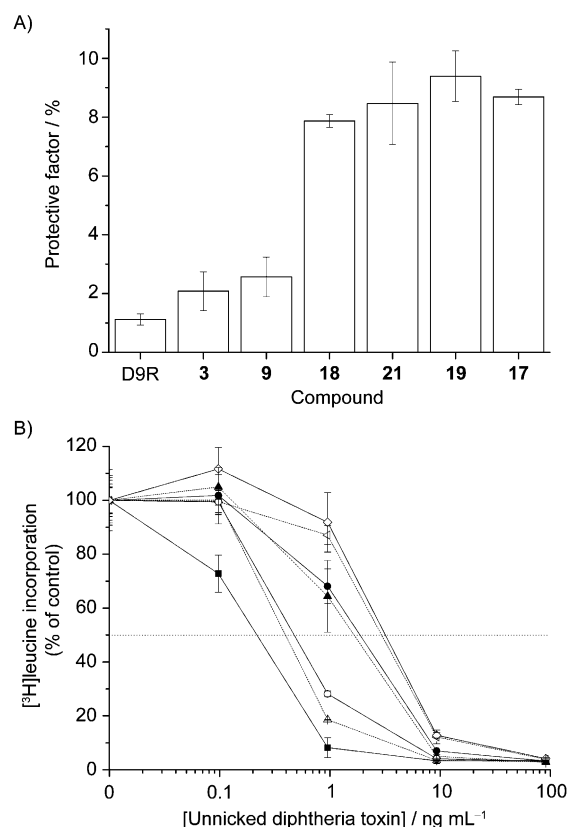


Figure 4. Intoxication of Vero cells by unnicked diphtheria toxin ($n=2$). A) Protection against diphtheria toxin by selected inhibitors (all at 100 nM final concentration); B) Concentration-dependent protection of cells by inhibitors **17** and **19** against 0.1 , 1 , 10 , and 100 ng mL^{-1} of unnicked diphtheria toxin [control without inhibitor (\blacksquare), $\text{ID}_{50}=0.23 \text{ ng mL}^{-1}$; inhibitor **17**: 2 nM (\triangle), $\text{ID}_{50}=0.41 \text{ ng mL}^{-1}$; 10 nM (\blacktriangle), $\text{ID}_{50}=1.75 \text{ ng mL}^{-1}$; 50 nM (\triangleleft), $\text{ID}_{50}=3.13 \text{ ng mL}^{-1}$; inhibitor **19**: 2 nM (\circ), $\text{ID}_{50}=0.49 \text{ ng mL}^{-1}$; 10 nM (\bullet), $\text{ID}_{50}=1.98 \text{ ng mL}^{-1}$, and 50 nM (\diamond), $\text{ID}_{50}=3.38 \text{ ng mL}^{-1}$; ID_{50} =half maximal infectious dose].

dues showed significantly stronger protection. The best results were achieved with Tle derivative **19** and Val analogue **17**, both containing guanidinomethyl substitution in the *para* position of the P5 phenyl ring. The protection factors determined for inhibitors **19** and **17** are 9.39 ± 0.86 and 8.69 ± 0.26 , respectively. On the basis of this prescreen, a second experiment with varying concentrations of these two inhibitors was performed (Figure 4B). As expected, concentration-dependent protection was detected for both analogues, whereby at all concentrations a slightly better effect was found for Tle inhibitor **19**. Notably, all inhibitors tested provided no protection against already-nicked diphtheria toxin, which confirms that the intoxication depends on the proteolytic activation of the toxin.

Inhibition of influenza virus propagation

The HPAIVs induce severe systemic infections with multiorgan failure in birds, which leads to 75–100% mortality within 10 days. Owing to close contact with infected animals or contaminated environment, the virus can also infect humans with

a high mortality rate. However, no transmission of these strains among humans has been reported so far. Nevertheless, the HPAIV strains could acquire the potential to provoke pandemic flu by efficient transmission between humans.^[35] For the replication of influenza viruses, the trimeric hemagglutinin precursor protein (HA0) has to be cleaved by a host cell protease into the subunits HA1 and HA2.^[36] The HPAIV strains of subtypes H5 and H7 possess a multibasic cleavage site, which is activated by furin or the closely related PC5/6, and this makes these PCs attractive targets for antiviral therapy.^[37]

Therefore, selected inhibitors were investigated in a virus spread assay in MDCK II cells, which provides semiquantitative information about their influence on virus propagation. Also in these cells no significant cytotoxicity (< 10%) was observed at the used inhibitor concentrations (Figure S5). Cells were infected by the HPAIV strains A/FPV/Rostock/34 (H7N1) and A/Thailand/KAN-1/2004 (H5N1) at indicated inhibitor concentrations (Figure 5 A,B). After 24 h, immunostaining of the nucleoprotein indicates the efficacy of virus propagation, as described previously.^[38,39]

A nearly identical influence of the inhibitors was observed with both HPAIV strains. Compared to the control, the reference inhibitor D9R and **9** containing the neutral P5 residue showed no effect on virus spread at the used concentrations. An improved potency was found for inhibitor **18** containing a *p*-aminomethyl substituent at the P5 phenyl ring and Tle in the P3 position. Surprisingly, *m*-aminomethyl-substituted analogue **20** showed only a negligible effect. Similar to that found in the anthrax and diphtheria toxin assays, the best results were obtained again with Tle derivative **19** and Val-containing analogue **17** modified by an N-terminal *p*-guanidinomethyl substituent. Both compounds significantly reduced virus spread up to an inhibitor concentration of 5 μM .

Inhibition of canine distemper virus propagation

Canine distemper virus (CDV) belongs to the Paramyxoviridae family and is closely related to measles and to a lesser extent to mumps and parainfluenza viruses. In carnivores, its natural hosts, CDV causes a severe acute disease with high mortality and frequent neurologic complications. In the TGN, furin cleaves the precursor fusion protein F0 in the mature form consisting of disulfide bond linked subunits F1 and F2, which is a prerequisite for the fusion of the viral envelope with the plasma membrane of the target cell.^[40,41] The inhibition of furin or related PCs could thus be a suitable approach for the treatment of paramyxoviruses with furin-activated fusion proteins. To test this hypothesis, the effect of inhibitors **9**, **17**, **19**, and D9R on CDV propagation was examined in VeroSLAMdogtag cells^[42] by measuring the viral titers in the supernatant and in the cellular fractions on days 1, 2, and 3 after infection (Figure 6). The virus titers are expressed as the logarithmic value of the dilution factor, at which 50% of the wells show a cytopathic effect ($\log_{10} \text{TCID}_{50}$). For less effective inhibitors D9R and **9**, significantly reduced virus titers in the supernatant and the cellular fractions were only seen at the highest concentration of 50 μM . In contrast, more potent furin inhibitors

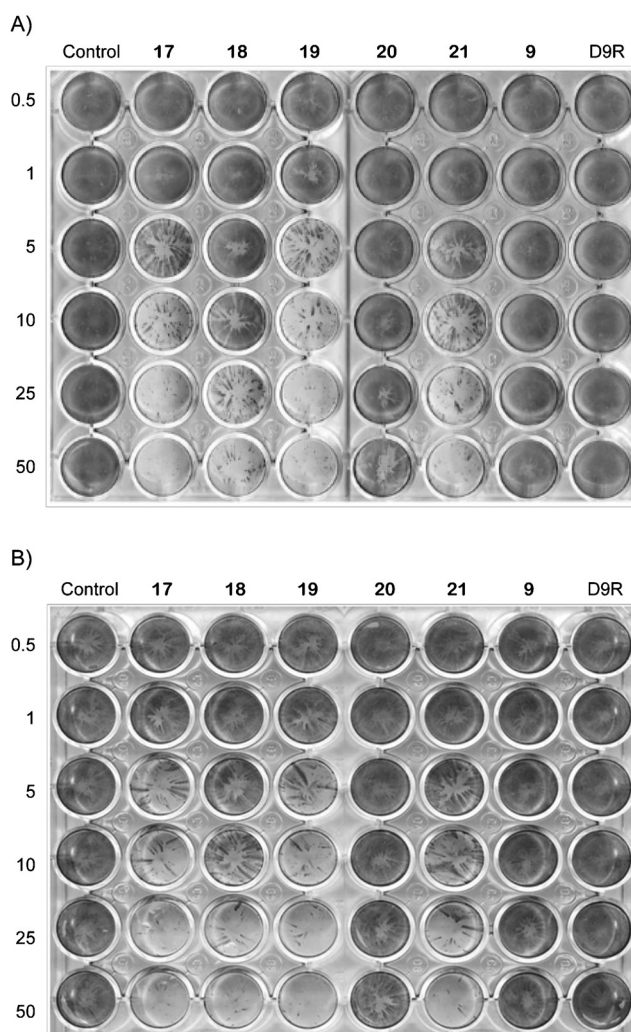


Figure 5. Suppression of influenza virus spread by selected furin inhibitors. MDCK II cells were infected with FPV (A) or KAN-1 virus (B) at an MOI of 0.001 and incubated without (control) or with various concentrations of indicated inhibitors. At 24 h post infection, the cells were immunostained with anti-FPV antibodies, whereas virus spread is indicated by gray spots.

17 and **19** with *p*-guanidinomethyl substitution at the P5 phenyl ring resulted in an antiviral effect starting at 0.5 μM .

Discussion

Upon starting our work on substrate-analogue furin inhibitors,^[17] we simply selected Val as the P3 residue, because it was known to be well suited for that position on the basis of various studies with peptidic chloromethyl ketones.^[43] In a second series, we tried to optimize the P3 position but could not identify a better residue. Nearly identical potency was found for an analogous Ile inhibitor, whereby the γ -branched Leu derivative was approximately 15-fold less potent.^[22] To increase our understanding of the influence of the P3 moiety, a new inhibitor series with nonproteinogenic residues was prepared. Very poor potency was found for Aib inhibitor **6**. From NMR spectroscopy studies with relatively short peptides it is known that relative to Ala, the additional $C\alpha$ substitution leads

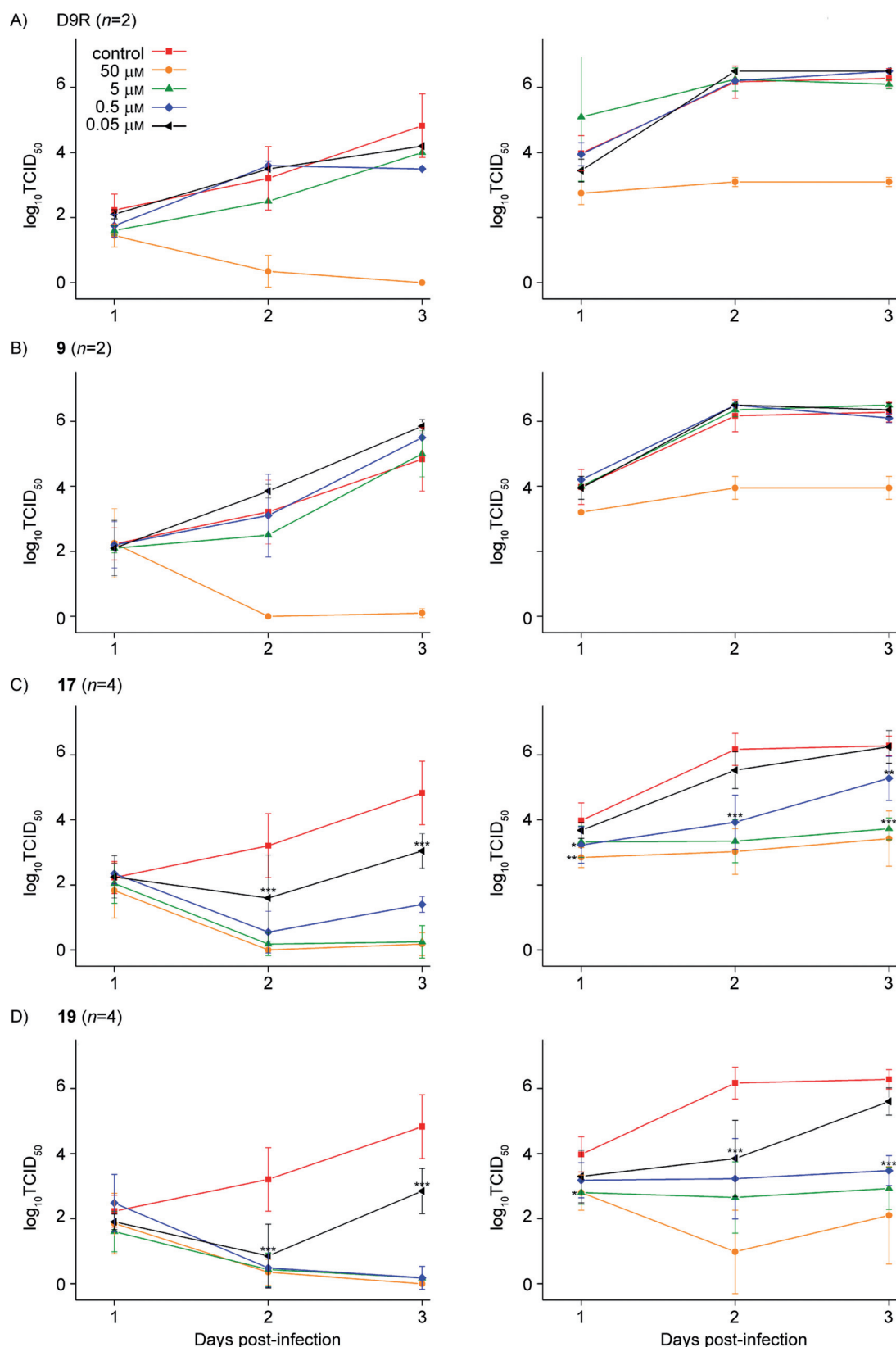


Figure 6. Infection of VeroSLAMdogtag cells with CDV in the presence of the indicated furin inhibitors A) D9R ($n=2$), B) 9 ($n=2$), C) 17 ($n=4$), and D) 19 ($n=4$) at various concentrations. The determined $\log_{10} \text{TCID}_{50}$ values of the cell-free titers (left) and the cell-associated titers (right) were determined 24, 48, and 72 h post infection. The significances (*, $P < 0.05$; **, $P < 0.01$, ***, $P < 0.001$) were calculated by the two-way analysis of variance (ANOVA) by using the Holm–Sidak method for multiple comparison versus a control group (without inhibitor) implemented in Sigmaplot 11.0.

to a further drastically reduced conformational space accessible for the Aib residue.^[44] In consequence, the ϕ and ψ torsion angles in Aib preferably adopt values found in helical structures, which should disturb the typical antiparallel β -sheet binding mode around the P3 residue determined for substrate-analogue inhibitors in complex with furin^[21,23] and other subtilisin- or chymotrypsin-like proteases.^[45,46]

In contrast, inhibitory potency was gradually improved by adding one, two, and three methyl groups to the C β atom of Ala, and the highest affinity was obtained for Tle inhibitor **9**. A similarly strong furin inhibition was found for related penicillamine inhibitor **15**, which suggests that the quaternary C β group provides a major binding contribution. In contrast, poor affinity was found for 1-Adg analogue **7**, the third inhibitor possessing this structural motif. Most likely, the sterically demanding adamantyl group prohibits proper binding of this inhibitor.

Interestingly, Tle is also used as the P3 residue in the approved hepatitis C virus (HCV) protease inhibitors boceprevir^[47] and telaprevir^[48] and is incorporated twice in the HIV protease inhibitor atazanavir.^[49] The *S* enantiomer of Tle is available in large quantities by reductive amination of trimethylpyruvic acid catalyzed by leucine dehydrogenase. Its bulky, space-filling *tert*-butyl side chain and concomitant hydrophobicity contributes to conformational control of peptide drugs and improves its overall stability against enzymatic degradation.^[50] A combination of spectroscopic studies revealed that tetrasubstitution at the C β atom preferentially leads to extended peptide conformations.^[51] Comparison of the new crystal structure of inhibitor **19** with the previously solved furin structures in complex with P3 Val analogues^[21] revealed that the terminal methyl groups of Val can be perfectly superimposed with two side-chain methyl groups found in the Tle structure. For the additional third methyl group in Tle, we could not identify any specific contact with furin that could easily explain the improved affinity. It is, however, involved in additional close intramolecular van der Waals contacts to the amide hydrogen atom (with a distance to the nitrogen of 3.1 Å) and to the carbonyl oxygen atom (3.5 Å) of the P2 Arg residue. Very similar intramolecular distances of the Tle side chain to the neighboring P2 residue were found in the crystal structure of boceprevir in complex with the HCV NS3-4A protease (PDB-ID: 2OC8).^[47] Furthermore, a similar fourfold improvement in the value of K_i was observed for a Tle derivative relative to its Val analogue during the development of boceprevir. These boceprevir results are reminiscent of the differences in potency found in our furin inhibitor series, which suggests similar binding contributions of the Tle residue.^[47] We speculate that these additional intramolecular contacts stabilize the β -sheet-like backbone conformation of the bound inhibitor, which thereby contributes to the enhancement in potency, or possibly by stabilizing a more suitable preformed conformation in solution. However, the fourfold-improved in vitro potency found for Tle inhibitor **9** over that of Val analogue **3** was not retained in generally more potent inhibitors **19** and **17** that contain the *p*-guanidinomethyl substituent at the P5 phenyl ring. This was surprising, because with most of our previously developed substrate-

analogue furin inhibitors we observed additive effects in potency upon replacing one of the P5 to P1 groups with a better-suited residue. It seems that the additional basic P5 anchor, which strongly improves the affinity of this inhibitor type, largely compensates for the beneficial effect of the P3 Tle substituent, found only in the weaker inhibitors with a neutral P5 group. Nevertheless, Tle derivative **19** is the most potent synthetic, reversible furin in vitro inhibitor identified thus far. Similar tendencies in structure-activity relationships were also found for the inhibition of PC1/3 and PC2, whereas PC2 was clearly less potently inhibited. In these studies, Tle derivative **19** was also the strongest inhibitor, which suggests a general beneficial effect of this P3 residue in PC inhibitors.

The evaluation of selected inhibitors in various cell culture assays revealed that the efficacy of the Tle inhibitors was slightly stronger than that of their direct Val counterparts in most cases (see pairs **9** versus **3** and **19** versus **17**). The best results were obtained with Tle inhibitors **19** and **21** and Val analogue **17**, all containing guanidinomethyl substitution at the P5 ring, which leads to K_i values $< 10 \mu\text{M}$. Most of the other reference compounds showed reduced efficacy in cell culture and in some cases no effect. The differences found in the in vitro furin inhibition nicely correlate with their efficacies in protecting cells against intoxication by anthrax and diphtheria toxins. Moreover, relative to the inhibitor concentrations of our previous studies with shiga toxin in HEp-2 cells,^[20] much lower inhibitor concentrations were sufficient to demonstrate significant protective effects in these assays. This is understandable for anthrax toxin, because the activation of PA is catalyzed by cell surface-bound furin, which should be easily accessible to exogenously added inhibitors. However, furin-catalyzed cleavage of diphtheria toxin occurs within the early endosomes. Similar to the situation described for the endocytotic entry of polybasic cell penetrating peptides or oligoarginine derivatives, we assume that these multibasic PC inhibitors initially accumulate on the acidic cell surface and that this is followed by endocytotic uptake.^[52-54]

Much higher inhibitor concentrations were required for inhibition of HPAIV spread in MDCK cells, for which the inhibitors must reach furin residing in the TGN to block hemagglutinin (HA) cleavage. Many polybasic compounds tend to accumulate within the early endosomes, which can be further sorted to the late endosomes and lysosomes for degradation by carriers back to the plasma membrane or to the TGN.^[55] Through the latter mechanism, it is likely that a certain amount of the inhibitors reaches furin anchored in the TGN.

Although the furin-catalyzed activation of the CDV F0 protein also occurs in the TGN, more pronounced efficacy of our inhibitors was seen against that virus, likely because its replication cycle is slower than that of influenza. For the best inhibitor, Tle derivative **19**, significantly reduced virus titers were determined at a concentration of only $0.5 \mu\text{M}$. The availability of a small animal pathogenesis model for CDV will thus enable us to immediately assess the in vivo efficacy of the next-generation furin inhibitors, designed to possess increased bioavailability. Because of the high structural conservation of paramyxovirus F proteins, human viruses with furin-activated cleavage

sites will likely be inhibited to a similar extent. In addition to measles and mumps viruses, which remain two of the most important causes of vaccine-preventable childhood deaths, this also includes the human parainfluenza and respiratory syncytial viruses, which play an important role in infant mortality as a result of respiratory infections and croup, considered predisposing factors for asthma and chronic respiratory disease in later life.

Our data from the CDV and HPAIV studies in cell culture demonstrate a significant advantage for compounds containing *p*-guanidinomethyl substitution at the P5 phenyl ring. In contrast, poor activity was observed for inhibitor **9** containing a neutral P5 group, although its *in vitro* K_i value of 0.17 nM should be sufficient for furin inhibition. Therefore, we assume that the major beneficial effect of the basic P5 residue is primarily related to improved transport of the exogenously added inhibitors to its target in the TGN.

In the design of small-molecule drugs designed both to bind to intracellular targets and to be orally available, it is a common strategy to use nonpeptidic structures and to avoid the presence or to reduce the number of highly charged groups such as guanidines or amidines. However, it will be challenging to achieve sufficient potency against furin-like PCs with neutral drug molecules, although a few of these possess micromolar potency.^[14,56,57] Moreover, although excellent amidine prodrugs have been developed,^[58] there is no or only little progress in the design of guanidine prodrugs.^[59] Therefore, it will likely be difficult to convert these tetrabasic inhibitors into completely neutral analogues on the basis of only prodrug strategies. All potent low-nanomolar furin inhibitors presently known possess several basic residues, and such compounds will be scarcely orally available. However, for parenteral application it might represent no disadvantage for inhibitors to possess more than two or three basic residues, especially given that prior studies of oligobasic cell penetrating peptides indicate enhanced cell entry.

Conclusions

In summary, identification of *tert*-leucine as the most suitable P3 residue provided highly potent furin inhibitors such as compound **19** (MI-1148). Incubation experiments of inhibitors **17** and **19** in human plasma over a period of 10 h also revealed the high stability of both compounds (see the Supporting Information). Inhibitor MI-1148 possesses strong antiviral activities in the used influenza and canine distemper virus propagation models in cell culture and strongly protects cells against anthrax and diphtheria toxins. Moreover, owing to their low picomolar potency we expect that this inhibitor scaffold will be able to tolerate a wide range of further modifications, which hopefully will improve bioavailability or selectivity within the PC family. Even after a strong drop in affinity it should still be possible to obtain nanomolar furin inhibitors with sufficient potency to be used as drug candidates to treat infectious diseases.

Experimental Section

Synthesis of inhibitors **18** and **19**

General: Analytical HPLC experiments were performed by using a Shimadzu LC-10A system (column: Nucleodur C₁₈, 5 μ m, 100 \AA , 4.6 \times 250 mm, Machery–Nagel, Düren, Germany) with a linear gradient of acetonitrile in water containing 0.1% trifluoroacetic acid (TFA, 1–50% acetonitrile in 49 min for all final inhibitors and 40–90% acetonitrile for protected intermediate **22**, detection at $\lambda = 220$ nm) at a flow rate of 1 mL min⁻¹. The final inhibitors were purified to more than 95% purity (based on detection at $\lambda = 220$ nm) by using preparative HPLC (pumps: Varian PrepStar Model 218 gradient system, detector: ProStar Model 320, fraction collector: Varian Model 701) by using a C₈ column (Nucleodur, 5 μ m, 100 \AA , 32 \times 250 mm, Machery–Nagel, Düren, Germany) and a linear gradient of acetonitrile containing 0.1% TFA at a flow rate of 20 mL min⁻¹. All peptides were finally obtained as TFA salts after lyophilization. The molecular mass of the synthesized compounds was determined by using a QTrap 2000 ESI spectrometer (Applied Biosystems, now Life Technologies, Carlsbad, CA). Elemental analyses were performed by using an Elementar Vario MICRO analyzer (Elementar Analysensysteme GmbH, Hanau, Germany). ¹H NMR and ¹³C NMR spectra were recorded by using a Jeol-ECX500 (Jeol Inc., Peabody, MA) and were referenced to internal solvent signals.

The reagents for synthesis, including the standard Fmoc-protected amino acids, coupling reagents, resins, and solvents were obtained from Orpegen, Bachem, Iris Biotech GmbH, Fluka, Acros, or Aldrich. 3- and 4-*tert*-butoxycarbonyl (Boc)-aminomethylphenylacetic acids were purchased from PolyPeptides.

4-Aminomethyl-Phac-Arg-Tle-Arg-4-amba-4 TFA (18): The synthesis was performed by manual standard Fmoc SPPS in a 200 mL reaction vessel with frit starting with Fmoc-Arg(Pbf)-2-chlorotrityl resin (2.5 g, 0.66 mmol g⁻¹). Fmoc deprotection was performed with 20% piperidine in DMF (5 and 20 min), Fmoc amino acids (4 equiv), hydroxybenzotriazole (HOBt, 4 equiv), and *N,N,N',N'*-tetramethyl-*O*-(1*H*-benzotriazol-1-yl)uronium hexafluorophosphate (HBTU, 4 equiv), and *N,N*-diisopropylethylamine (DIPEA, 8 equiv) were used for coupling. For the coupling of Boc-4-aminomethylphenylacetic acid only a twofold excess (i.e., 2 equiv) of the phenylacetic acid derivative, HOBt, and HBTU in the presence of DIPEA (4 equiv) was used. Protected peptide **22** (Scheme 2) was cleaved from the resin under mild acidic conditions (80 mL 1% TFA in CH₂Cl₂, 3 \times 30 min) at room temperature. The cleavage mixture was immediately neutralized with DIPEA after each step (3 \times 1 mL). The solvent was removed *in vacuo* (yellowish oil, HPLC: $t_R = 28.93$ min; MS calcd: $m/z = 1194.58$, m/z found: 1196.10 [$M+H$]⁺).

The oily intermediate was dissolved in DMF (80 mL) and treated at 0 °C with 4-aminobenzylamine-2HCl^[17] (365 mg, 1.65 mmol), 6-Cl-HOBt (840 mg, 4.95 mmol), benzotriazol-1-yl-*N*-oxytris(pyrrolidino)phosphonium hexafluorophosphate (PyBOP; 947 mg, 1.82 mmol), and DIPEA (861 μ L, 4.95 mmol). The mixture was stirred at 0 °C for 15 min and then at room temperature overnight. The solvent was removed *in vacuo*, and the remaining intermediate was treated with TFA/triisopropylsilane (TIS)/H₂O (95:2.5:2.5 v/v/v, 20 mL) and stirred for 3 h at room temperature. The mixture was precipitated in cold diethyl ether, and owing to incomplete 2,2,4,6,7-pentametyldihydrobenzofuran-5-sulfonyl (Pbf) removal, the cleavage procedure was repeated. The crude intermediate was precipitated in diethyl ether and dried. The precipitate was purified by using preparative HPLC and was lyophilized from water to afford a white solid; yield: 1.23 g (63.2% based on initial resin loading); ¹H NMR

(500 MHz, [D₆]DMSO): δ = 0.87 (s, 9H), 1.34–1.64 (m, 6H), 1.64–1.76 (m, 2H), 2.98–3.17 (m, 4H), 3.45–3.58 (m, 2H), 4.00 (s, 2H), 4.16–4.39 (m, 4H), 4.44 (dd, J = 16.0, 6.3 Hz, 1H), 6.82–7.62 (m, 15H), 7.71–7.87 (m, 4H), 8.12 (d, J = 7.5 Hz, 1H), 8.23 (br. s., 3H), 8.41 (d, J = 8.0 Hz, 1H), 8.6 (t, J = 6.16 Hz, 1H), 9.17–9.42 ppm (m, 4H); ¹³C NMR (125 MHz, [D₆]DMSO): δ = 25.05, 25.14, 26.5, 28.6, 28.7, 34.3, 40.3, 40.4, 41.5, 41.7, 42.0, 52.3, 52.5, 59.5, 126.4, 127.2, 127.9, 128.6, 129.2, 132.0, 136.6, 145.7, 156.8, 165.4, 169.8, 170.2, 171.0, 171.4 ppm; MS: m/z (%): 722.1 [M+H]⁺; elemental analysis calcd (%) for C₄₃H₅₉F₁₂N₃O₁₂ (1178.00 g mol⁻¹): C 43.84, H 5.05, N 15.46; found: C 42.83, H 5.25, N 15.19; HPLC (λ = 220 nm): t_R = 19.12 min, purity: 96.9%.

4-Guanidinomethyl-Phac-Arg-Tle-Arg-4-amba-4 TFA (19): Inhibitor **18** (1 g, 0.85 mmol) was dissolved in 1 M Na₂CO₃ (10 mL) and DMF (5 mL). The mixture was treated with 1*H*-pyrazole-1-carboxamide-HCl (1.25 g, 8.5 mmol) and stirred at room temperature. After 7 h, the reaction was complete, and the mixture was acidified by the addition of TFA (pH \approx 3). The crude product was purified by preparative HPLC, and the product was lyophilized from water to afford a white solid; yield: 650 mg (0.533 mmol); ¹H NMR (500 MHz, [D₆]DMSO) δ = 0.86 (s, 9H), 1.37–1.63 (m, 6H), 1.63–1.76 (m, 2H), 3.00–3.17 (m, 4H), 3.43–3.56 (m, 2H), 4.20–4.39 (m, 6H), 4.44 (dd, J = 16.18, 6.16 Hz, 1H), 6.76–7.62 (m, 19H), 7.72–7.83 (m, 4H), 8.07–8.18 (m, 2H), 8.41 (d, J = 8.02 Hz, 1H), 8.56–8.64 (m, 1H), 9.21–9.41 ppm (m, 4H); ¹³C NMR (125 MHz, [D₆]DMSO) δ = 25.1, 25.2, 26.5, 28.5, 28.7, 34.3, 40.3, 40.4, 41.5, 41.7, 43.7, 52.3, 52.5, 59.5, 126.5, 127.1, 127.2, 127.9, 129.2, 135.2, 135.5, 145.7, 156.8, 156.9, 165.4, 169.8, 170.4, 171.0, 171.4 ppm; MS: m/z (%): 764.35 [M+H]⁺; elemental analysis calcd (%) for C₄₄H₆₁F₁₂N₃O₁₂ (1220.03 g mol⁻¹): C 43.32, H 5.04, N 17.22; found: C 42.21, H 5.31, N 17.07; HPLC: t_R = 20.41 min, purity: 97%.

The other inhibitors were prepared by an identical strategy;^[17,20,22] for the analytical data see Table 1.

Enzyme-based assays

Enzyme kinetic measurements with recombinant soluble human furin: The measurements were performed in black 96-well plates (Nunc, Langensfeld) at room temperature with a microplate reader (Safire², Tecan, Switzerland) at λ_{ex} = 380 nm and λ_{em} = 460 nm. Each well contained 2 μ L inhibitor solution (dissolved in DMSO), 20 μ L of Phac-Arg-Val-Arg-Arg-AMC as substrate (dissolved in water, concentrations used in the assay: 5, 20 and 50 μ M) and 160 μ L buffer [100 mM 4-(2-hydroxyethyl)-1-piperazineethanesulfonic acid (HEPES), 0.2% Triton X-100, 2 mM CaCl₂, 0.02% NaN₃, and 1 mg mL⁻¹ bovine serum albumin (BSA), pH 7.0]. The measurements were started by the addition of furin^[15] (20 μ L) solution. For inhibitors with neutral P5 residues, the lowest inhibitor concentration in the assay was 10 times higher than the enzyme concentration. The measurements were performed for 30 min, and the steady-state rates were calculated from the slopes of the progress curves. The K_i values were obtained by fitting the data to the equation for classical reversible competitive inhibition, as described previously.^[17] All data calculations were performed with Origin 8.1.

For tight-binding inhibitors with basic P5 residues Equation (1)^[60] was used, in which v_0 is the velocity in the absence of an inhibitor, I_t is the total inhibitor concentration, E_t is the total enzyme concentration, and K_i^* is the apparent inhibition constant at the used substrate concentration.

$$v = v_0 \times \frac{[(K_i^* + I_t - E_t)^2 + 4 \times K_i^* \times E_t]^{1/2} - (K_i^* + I_t - E_t)}{2 \times E_t} \quad (1)$$

The apparent K_i^* was converted into the true K_i by using Equation (2):

$$K_i = \frac{K_i^*}{1 + \frac{s}{K_M}} \quad (2)$$

Enzyme kinetic measurements with mPC1/3 and mPC2: The measurements were performed in 96-well plates (Costar Corning 3365) at 37 °C with a microplate reader (SpectraMaxM2, λ_{ex} = 380 nm and λ_{em} = 460 nm, Molecular Devices, LLC, Sunnyvale, CA). Each well contained 40 μ L of enzyme solution (for PC1/3:^[61] \approx 100 ng well⁻¹ in 100 mM sodium acetate buffer pH 5.5, containing 5 mM CaCl₂, 0.1% Brij 35, 0.1% NaN₃, and 0.01% BSA; for PC2:^[62] \approx 40 ng well⁻¹ in 100 mM sodium acetate buffer at pH 5, containing 2 mM CaCl₂, 0.1% Brij 35, 0.1% NaN₃, and 0.01% BSA). After the addition of inhibitor (5 μ L), dissolved in the aforementioned buffers, the plate was incubated for 20 min at room temperature. Then, the substrate Pyr-RTKR-AMC (5 μ L, Bachem, Bubendorf, Switzerland) dissolved in water (200 μ M in the assay) was added to provide a total assay volume of 50 μ L. The release of free fluorescent 7-amino-4-methylcoumarin (AMC) was measured over 30 min, and the slopes of the progress curves were calculated by linear regression.

Expression, crystallization, and structure determination: Expression, purification of human furin, and its crystallization in complex with inhibitor I-1 (*m*-guanidinomethyl-Phac-Arg-Val-Arg-4-amidinobenzylamid) were performed as previously described.^[21] Shortly, the protease was expressed by transient transfection of human embryonic kidney cells. Three chromatography steps including immobilized metal affinity purification, immobilized inhibitor affinity chromatography, and gel-permeation chromatography were applied for the purification of furin.

Initially, crystals of human furin were grown in complex with I-1. These crystals were washed with the crystallization solution (5 \times 0.5 μ L) supplemented with 1 mM of compound **19** and were finally soaked for 3 days. The crystals were transferred to soaking solution supplemented with 15% ethylene glycol, flash cooled in liquid nitrogen, and used for diffraction data collection at the BESSY-II beamline 14.1 of the Helmholtz-Zentrum Berlin (HZB).^[63] Data processing was performed with XDS^[64] (v.03/2013) and programs of the CCP4-suite^[65] (CCP4 v.6.3.0, CCP4 interface v.2.2.0). The R_{free} set of reflections was defined in thin shells with the DATAMAN software.^[66] CNS (v.1.3)^[67] was used for initial rigid body refinement with the structure of human furin (PDB-ID 4OMC^[21]). Model building was performed with COOT (v.0.6.2).^[68] CNS (v.1.3) was used for refinement by applying tight NCS restraints to the main chain atoms of the protein. Refinement parameters of the *p*-guanidinomethyl-Phac, Tle, and 4-amba moieties of the inhibitor, including bond length, bond angles, dihedrals, and force constants, were derived from small-molecule structures of the Cambridge structural database.^[69] MOLEMAN^[70] was used for analysis of B-factors. Kicked omit maps were calculated in PHENIX.^[71] PYMOL (<http://www.pymol.org>) was used for molecular graphics and structural alignments. Surface electrostatics were calculated with APBS^[72] and were visualized with the APBS PYMOL plugin.

Thermal denaturation assays: Thermal denaturation analysis (also called thermoflour or thermal shift assay^[26]) was performed in 40 mM sodium borate, pH 7.5, 100 mM NaCl, 2 mM CaCl₂, and 15 \times Sypro-Orange (Life Technologies), adding 1.5 μ M of the protease

and 5 μM of the inhibitors. The final reaction volume was 25 μL . Melting curves were determined with an IQ5 realtime PCR cycler (Biorad) by measuring the increase in the fluorescence at excitation and emission wavelengths of 490 and 575 nm, respectively. Heating was performed in 0.5 $^{\circ}\text{C}$ steps with a subsequent dwell time of 15 s. The melting temperatures correspond to the inflection points of the melting curves, which were determined with the data analysis module of the IQ5 software (Bio-Rad, v2.1.97.1001). All measurements were performed in triplicate.

Assays in cell culture

Inhibition of anthrax toxin action: Murine macrophage J774A.1 cells (200 μL , 5×10^5 cells mL^{-1} ; German collection of microorganisms and cell cultures, Braunschweig, Germany) were grown overnight in wells of a 96-well plate (Becton Dickinson Labware, Heidelberg) by using Roswell Park Memorial Institute (RPMI) medium/Dulbecco's modified Eagle's medium (DMEM) (1:1) containing 10% fetal calf serum (FCS) at 37 $^{\circ}\text{C}$ and 5% CO_2 as a seeding medium. Then the cells were treated with a prepared solution of protective antigen (PA, 500 ng mL^{-1} in assay), lethal factor (LF, 100 ng mL^{-1} in assay), and various inhibitor concentrations (0.05–100 μM in the assay) dissolved in sample medium containing 95% DMEM and 5% FCS. PA and LF were obtained from List Biological Laboratories, Inc., Campbell, USA. The cells were incubated at 37 $^{\circ}\text{C}$ and 5% CO_2 for 3 h. Afterwards, 25 μL of 3-(4,5-dimethylthiazol-2-yl)-2,5-diphenyltetrazolium bromide (MTT) solution [5 mg mL^{-1} in phosphate-buffered saline (PBS)] was added to each well, and the cells were incubated in the dark at 37 $^{\circ}\text{C}$ with 5% CO_2 for 2 h. After cell lysis with 90% isopropanol (v/v, 100 μL), 0.5% sodium dodecyl sulfate (SDS) (w/v), and 25 mM HCl, the absorbance of each well was measured by using a microplate reader (Model 680, Biorad Laboratories, Hercules, CA) at $\lambda = 540$ nm.^[73] The resulting measurements were normalized through subtraction of the mean of the blanks (no cells, sample medium with toxin). The protection was estimated as a percentage of the medium control (cells with sample medium devoid of toxin) with the toxin control (cells with sample medium and toxin) as zero value [protection = (sample – toxin control) / (medium control – toxin control) \times 100].

Inhibition of diphtheria toxin action: The Vero cells used were maintained in DMEM.^[74] The cells were seeded into 24-well plates at a density of 5×10^4 cells well^{-1} 1 day before the experiment. The cells were preincubated with or without the inhibitors (100 nM in the prescreen and 2, 10, and 50 nM in case of the concentration dependency) in leucine-free and serum-free medium for 30 min, followed by the addition of various concentrations of unlicked diphtheria toxin (Merck KGaA, Darmstadt, Germany; 0.1, 1, 10, and 100 ng mL^{-1} in the assay). After 3 h, the cells were incubated in HEPES medium containing 1 $\mu\text{Ci mL}^{-1}$ [^3H]leucine (Hartmann Analytic, Braunschweig, Germany) without unlabeled leucine for 20 min. Then, the medium was removed, the cells were washed with 5% trichloroacetic acid (2 \times), dissolved in 0.1 M KOH, and the radioactivity was measured.

Inhibition of influenza virus propagation: MDCK II cells were seeded in 24-well plates and grown to 100% confluency. Cells were infected with A/FPV/Rostock/34 (H7N1) or A/Thailand/1(KAN-1)/2004 (H5N1) at a multiplicity of infection (MOI) of 0.001 at 37 $^{\circ}\text{C}$ for 1 h. After that, virus-containing media were removed and cells were washed with PBS pH 7.0.^[39] Fresh media containing inhibitors at indicated concentrations were added to the cells. Cells were incubated in the presence and absence of inhibitors for 24 h at 37 $^{\circ}\text{C}$. Infected cells were immunostained by using anti-FPV-antibodies.

Inhibition of canine distemper virus propagation: VeroSLAMdogtag cells^[42] were seeded in 12-well plates at 80% confluency. Eight hours prior to infection, the culture medium was changed to DMEM media containing the respective inhibitor at the appropriate concentration or untreated medium. Cells were then infected with CDV 5804PeH^[27] at a MOI of 0.01, and supernatant and cell-associated samples were collected every 24 h for 3 days. The medium of all wells was changed daily to assure the presence of the inhibitor throughout the experiment. Titers were quantified by using the limited dilution method and are expressed as 50 tissue culture infectious doses (TCID₅₀).

Acknowledgements

The work of W.G. was supported by the Collaborative Research Centre 593 of the German Research Foundation (DFG).

Keywords: antiviral agents • crystal structure analysis • furin • inhibitors • proprotein convertases

- [1] G. Thomas, *Nat. Rev. Mol. Cell Biol.* **2002**, *3*, 753–766.
- [2] N. G. Seidah, A. Prat, *Nat. Rev. Drug Discovery* **2012**, *11*, 367–383.
- [3] A. J. Roebroek, L. Umans, I. G. Pauli, E. J. Robertson, F. van Leuven, W. J. Van de Ven, D. B. Constam, *Development* **1998**, *125*, 4863–4876.
- [4] J. W. Creemers, A. M. Khatib, *Front. Biosci.* **2008**, 4960–4971.
- [5] A. J. Roebroek, N. A. Taylor, E. Louagie, I. Pauli, L. Smeijers, A. Snellinx, A. Lauwers, W. J. Van de Ven, D. Hartmann, J. W. Creemers, *J. Biol. Chem.* **2004**, *279*, 53442–53450.
- [6] M. S. Sarac, A. Cameron, I. Lindberg, *Infect. Immun.* **2002**, *70*, 7136–7139.
- [7] M. S. Sarac, J. R. Peinado, S. H. Leppla, I. Lindberg, *Infect. Immun.* **2004**, *72*, 602–605.
- [8] F. Couture, F. D'Anjou, R. Day, *Biomol. Concepts* **2011**, *2*, 421–438.
- [9] A. Pasquato, J. Ramos da Palma, C. Galan, N. G. Seidah, S. Kunz, *Antiviral Res.* **2013**, *99*, 49–60.
- [10] N. Senzer, M. Barve, J. Kuhn, A. Melnyk, P. Beitsch, M. Lazar, S. Lifshitz, M. Magee, J. Oh, S. W. Mill, C. Bedell, C. Higgs, P. Kumar, Y. Yu, F. Norvell, C. Phalon, N. Taquet, D. D. Rao, Z. Wang, C. M. Jay, B. O. Pappen, G. Wallraven, F. C. Brunicardi, D. M. Shanahan, P. B. Maples, J. Nemunaitis, *Mol. Ther.* **2012**, *20*, 679–686.
- [11] N. Senzer, M. Barve, J. Nemunaitis, J. Kuhn, A. Melnyk, P. Beitsch, M. Magee, J. Oh, C. Bedell, P. Kumar, D. D. Rao, B. O. Pappen, G. Wallraven, C. Brunicardi, P. B. Maples, J. Nemunaitis, *J. Vaccines Vaccin.* **2013**, *4*, 209.
- [12] J. Nemunaitis, M. Barve, D. Orr, J. Kuhn, M. Magee, J. Lamont, C. Bedell, G. Wallraven, B. O. Pappen, A. Roth, S. Horvath, D. Nemunaitis, P. Kumar, P. B. Maples, N. Senzer, *Oncology* **2014**, *87*, 21–29.
- [13] A. Basak, *J. Mol. Med.* **2005**, *83*, 844–855.
- [14] U. C. De, P. Mishra, P. R. Pal, B. Dinda, A. Basak, *Colloquium Series on Protein Activation and Cancer* **2012**, *1*, 1–76.
- [15] M. M. Kacprzak, J. R. Peinado, M. E. Than, J. Appel, S. Henrich, G. Lipkind, R. A. Houghten, W. Bode, I. Lindberg, *J. Biol. Chem.* **2004**, *279*, 36788–36794.
- [16] G. S. Jiao, L. Cregar, J. Wang, S. Z. Millis, C. Tang, S. O'Malley, A. T. Johnson, S. Sareth, J. Larson, G. Thomas, *Proc. Natl. Acad. Sci. USA* **2006**, *103*, 19707–19712.
- [17] G. L. Becker, F. Sielaff, M. E. Than, I. Lindberg, S. Routhier, R. Day, Y. Lu, W. Garten, T. Steinmetzer, *J. Med. Chem.* **2010**, *53*, 1067–1075.
- [18] H. Gagnon, S. Beauchemin, A. Kwiatkowska, F. Couture, F. D'Anjou, C. Levesque, F. Dufour, A. R. Desbiens, R. Vaillancourt, S. Bernard, R. Desjardins, F. Malouin, Y. L. Dory, R. Day, *J. Med. Chem.* **2014**, *57*, 29–41.
- [19] A. Kwiatkowska, F. Couture, C. Levesque, K. Ly, R. Desjardins, S. Beauchemin, A. Prah, B. Lammek, W. Neugebauer, Y. L. Dory, R. Day, *J. Med. Chem.* **2014**, *57*, 98–109.

- [20] G. L. Becker, Y. Lu, K. Harges, B. Strehlow, C. Levesque, I. Lindberg, K. Sandvig, U. Bakowsky, R. Day, W. Garten, T. Steinmetzer, *J. Biol. Chem.* **2012**, *287*, 21992–22003.
- [21] S. O. Dahms, K. Harges, G. L. Becker, T. Steinmetzer, H. Brandstetter, M. E. Than, *ACS Chem. Biol.* **2014**, *9*, 1113–1118.
- [22] G. L. Becker, K. Harges, T. Steinmetzer, *Bioorg. Med. Chem. Lett.* **2011**, *21*, 4695–4697.
- [23] S. Henrich, A. Cameron, G. P. Bourenkov, R. Kiefersauer, R. Huber, I. Lindberg, W. Bode, M. E. Than, *Nat. Struct. Biol.* **2003**, *10*, 520–526.
- [24] M. S. Bernatowicz, Y. Wu, G. R. Matsueda, *J. Org. Chem.* **1992**, *57*, 2497–2502.
- [25] G. N. Ramachandran, V. Sasisekharan, *Adv. Protein Chem.* **1968**, *23*, 283–438.
- [26] U. B. Ericsson, B. M. Hallberg, G. T. Detitta, N. Dekker, P. Nordlund, *Anal. Biochem.* **2006**, *357*, 289–298.
- [27] V. von Messling, D. Milosevic, R. Cattaneo, *Proc. Natl. Acad. Sci. USA* **2004**, *101*, 14216–14221.
- [28] T. C. Dixon, M. Meselson, J. Guillemin, P. C. Hanna, *N. Engl. J. Med.* **1999**, *341*, 815–826.
- [29] S. Liu, M. Moayeri, S. H. Leppla, *Trends Microbiol.* **2014**, *22*, 317–325.
- [30] J. A. Young, R. J. Collier, *Annu. Rev. Biochem.* **2007**, *76*, 243–265.
- [31] A. W. Arstenstein, S. M. Opal, *Clin. Infect. Dis.* **2012**, *54*, 1148–1161.
- [32] S. Mazumdar, *MAbs* **2009**, *1*, 531–538.
- [33] T. L. Hadfield, P. McEvoy, Y. Polotsky, V. A. Tzinslerling, A. A. Yakovlev, *J. Infect. Dis.* **2000**, *181*, S116–S120.
- [34] M. Tsuneoka, K. Nakayama, K. Hatsuzawa, M. Komada, N. Kitamura, E. Mekada, *J. Biol. Chem.* **1993**, *268*, 26461–26465.
- [35] C. J. Russell, R. G. Webster, *Cell* **2005**, *123*, 368–371.
- [36] H. D. Klenk, W. Garten, *Trends Microbiol.* **1994**, *2*, 39–43.
- [37] W. Garten, H. D. Klenk in *Avian Influenza*, Vol. 27 (Eds.: H. D. Klenk, M. Matrosovich, J. Stech), Karger, Basel, **2008**, pp. 156–167.
- [38] E. Böttcher, C. Freuer, T. Steinmetzer, H. D. Klenk, W. Garten, *Vaccine* **2009**, *27*, 6324–6329.
- [39] E. Böttcher-Friebertshäuser, C. Freuer, F. Sielaff, S. Schmidt, M. Eickmann, J. Uhlendorff, T. Steinmetzer, H. D. Klenk, W. Garten, *J. Virol.* **2010**, *84*, 5605–5614.
- [40] V. von Messling, D. Milosevic, P. Devaux, R. Cattaneo, *J. Virol.* **2004**, *78*, 7894–7903.
- [41] A. Beineke, C. Puff, F. Seehusen, W. Baumgartner, *Vet. Immunol. Immunopathol.* **2009**, *127*, 1–18.
- [42] V. von Messling, C. Springfield, P. Devaux, R. Cattaneo, *J. Virol.* **2003**, *77*, 12579–12591.
- [43] W. Garten, S. Hallenberger, D. Ortmann, W. Schäfer, M. Vey, H. Angliker, E. Shaw, H. D. Klenk, *Biochimie* **1994**, *76*, 217–225.
- [44] S. Raghothama, M. Chaddha, P. Balaram, *Proc. Natl. Acad. Sci., India, Sect. A* **1996**, *66*, 33–44.
- [45] J. J. Perona, C. S. Craik, *Protein Science* **1995**, *4*, 337–360.
- [46] P. K. Madala, J. D. Tyndall, T. Nall, D. P. Fairlie, *Chem. Rev.* **2010**, *110*, PR1–PR31.
- [47] S. Venkatraman, S. L. Bogen, A. Arasappan, F. Bennett, K. Chen, E. Jao, Y. T. Liu, R. Lovey, S. Hendrata, Y. Huang, W. Pan, T. Parekh, P. Pinto, V. Popov, R. Pike, S. Ruan, B. Santhanam, B. Vibulbhan, W. Wu, W. Yang, J. Kong, X. Liang, J. Wong, R. Liu, N. Butkiewicz, R. Chase, A. Hart, S. Agrawal, P. Ingravallo, J. Pichardo, R. Kong, B. Baroudy, B. Malcolm, Z. Guo, A. Prongay, V. Madison, L. Broske, X. Cui, K. C. Cheng, Y. Hsieh, J. M. Brisson, D. Prelusky, W. Korfmacher, R. White, S. Bogdanowich-Knipp, A. Pavlovsky, P. Bradley, A. K. Saksena, A. Ganguly, J. Piwinski, V. Girijavallabhan, F. G. Njoroge, *J. Med. Chem.* **2006**, *49*, 6074–6086.
- [48] S.-H. Chen, S.-L. Tan, *Curr. Med. Chem.* **2005**, *12*, 2317–2342.
- [49] B. S. Robinson, K. A. Riccardi, Y. F. Gong, Q. Guo, D. A. Stock, W. S. Blair, B. J. Terry, C. A. Deminie, F. Djang, R. J. Colonna, P. F. Lin, *Antimicrob. Agents Chemother.* **2000**, *44*, 2093–2099.
- [50] A. S. Bommarium, M. Schwarm, K. Stingl, M. Kottenhahn, K. Huthmacher, K. Drauz, *Tetrahedron: Asymmetry* **1995**, *6*, 2851–2888.
- [51] F. Formaggio, C. Baldini, V. Moretto, M. Crisma, B. Kaptein, Q. B. Broxterman, C. Toniolo, *Chem. Eur. J.* **2005**, *11*, 2395–2404.
- [52] S. M. Fuchs, R. T. Raines, *Cell. Mol. Life Sci.* **2006**, *63*, 1819–1822.
- [53] F. Milletti, *Drug Discovery Today* **2012**, *17*, 850–860.
- [54] S. Katayama, H. Hirose, K. Takayama, I. Nakase, S. Futaki, *J. Controlled Release* **2011**, *149*, 29–35.
- [55] B. D. Grant, J. G. Donaldson, *Nat. Rev. Mol. Cell Biol.* **2009**, *10*, 597–608.
- [56] T. Komiyama, J. M. Coppola, M. J. Larsen, M. E. van Dort, B. D. Ross, R. Day, A. Rehemtulla, R. S. Fuller, *J. Biol. Chem.* **2009**, *284*, 15729–15738.
- [57] J. M. Coppola, M. S. Bhojani, B. D. Ross, A. Rehemtulla, *Neoplasia* **2008**, *10*, 363–370.
- [58] P. Ettmayer, G. L. Amidon, B. Clement, B. Testa, *J. Med. Chem.* **2004**, *47*, 2393–2404.
- [59] D. Schade, J. Kotthaus, L. Riebling, H. Müller-Fielitz, W. Raasch, O. Koch, N. Seidel, M. Schmidtke, B. Clement, *J. Med. Chem.* **2014**, *57*, 759–769.
- [60] J. W. Williams, J. F. Morrison, *Methods Enzymol.* **1979**, *63*, 437–467.
- [61] Y. Zhou, I. Lindberg, *J. Biol. Chem.* **1993**, *268*, 5615–5623.
- [62] N. S. Lamango, X. Zhu, I. Lindberg, *Arch. Biochem. Biophys.* **1996**, *330*, 238–250.
- [63] U. Mueller, N. Darowski, M. R. Fuchs, R. Forster, M. Hellmig, K. S. Paithankar, S. Puhlinger, M. Steffien, G. Zocher, M. S. Weiss, *J. Synchrotron Radiat.* **2012**, *19*, 442–449.
- [64] W. Kabsch, *Acta Crystallogr. Sect. D* **2010**, *66*, 125–132.
- [65] M. D. Winn, C. C. Ballard, K. D. Cowtan, E. J. Dodson, P. Emsley, P. R. Evans, R. M. Keegan, E. B. Krissinel, A. G. Leslie, A. McCoy, S. J. McNicholas, G. N. Murshudov, N. S. Pannu, E. A. Potterton, H. R. Powell, R. J. Read, A. Vagin, K. S. Wilson, *Acta Crystallogr. Sect. D* **2011**, *67*, 235–242.
- [66] G. J. Kleywegt, T. A. Jones, *Acta Crystallogr. Sect. D* **1996**, *52*, 826–828.
- [67] A. T. Brunger, *Nat. Protoc.* **2007**, *2*, 2728–2733.
- [68] P. Emsley, B. Lohkamp, W. G. Scott, K. Cowtan, *Acta Crystallogr. Sect. D* **2010**, *66*, 486–501.
- [69] F. H. Allen, *Acta Crystallogr. Sect. B* **2002**, *58*, 380–388.
- [70] G. J. Kleywegt, *J. Mol. Biol.* **1997**, *273*, 371–376.
- [71] P. D. Adams, P. V. Afonine, G. Bunkoczi, V. B. Chen, I. W. Davis, N. Echols, J. J. Headd, L. W. Hung, G. J. Kapral, R. W. Grosse-Kunstleve, A. J. McCoy, N. W. Moriarty, R. Oeffner, R. J. Read, D. C. Richardson, J. S. Richardson, T. C. Terwilliger, P. H. Zwart, *Acta Crystallogr. Sect. D* **2010**, *66*, 213–221.
- [72] N. A. Baker, D. Sept, S. Joseph, M. J. Holst, J. A. McCammon, *Proc. Natl. Acad. Sci. USA* **2001**, *98*, 10037–10041.
- [73] T. Mosmann, *J. Immunol. Methods* **1983**, *65*, 55–63.
- [74] A. Kurmanova, A. Llorente, A. Polesskaya, O. Garred, S. Olsnes, J. Kozlov, K. Sandvig, *Biochem. Biophys. Res. Commun.* **2007**, *357*, 144–149.

Received: March 5, 2015

Published online on May 14, 2015